Design and Operation of a 150 W Near Diffraction-Limited Laser Amplifier with SBS Wavefront Correction

C. B. Dane, L. E. Zapata, W. A. Neuman, M. A. Norton, and L. A. Hackel

Abstract—**The design and operation of a Nd:glass regenerative amplifier using a stimulated Brillouin scattering (SBS) phase conjugate mirror is presented. The system can be operated at 25–30 J per pulse with a pulse width of 14 ns and a pulse repetition frequency (PRF) of 6 Hz. This results in an average output power of >150 W with a peak power of 2 GW. The experimentally measured divergence of the amplifier output is 1.25× the diffraction limit and it can be frequency doubled with >80% efficiency. The detailed considerations required for this specific amplifier design are discussed as well as how these considerations apply to the design of high average power, high beam quality laser systems in general.**

I. Introduction

FOR certain applications of high average power solid state lasers, it is desirable to extract a relatively large stored energy in a laser pulse from a single amplifier aperture. Examples of these are the production of x-rays for photolithography [1], the generation of artificial pulsed laser guide stars [2], and the illumination of targets for speckle interferometric imaging. Although the Nd:glass gain medium exhibits a lower fracture strength and thermal conductivity than crystalline materials such as Nd:YAG, its availability in large volumes and its small cross section for stimulated emission (3.5×10^{-20} cm^2) make it well suited to the storage requirements of high energy per pulse operation. We have developed a high beam quality flashlamp pumped Nd:glass amplifier system with an output energy of 25–30 J/pulse in 14 ns and with an average output power of 150 W. The use of an SBS phase conjugate mirror in the optical system produces a smooth near field beam distribution with a measured divergence that is 1.25× the diffraction limit.

Since the conception of the face-pumped, zig-zag path slab laser [3], it has undergone an extensive amount of investigation and development. Reference [4] presents a valuable summary of the developmental history of the slab architecture as well as examples of many actual implementations in working laser systems. Notable early work on the subject [5]–[7] remains important in our present understanding of the performance potentials as well as limitations of zig-zag slab designs and has provided an important foundation for much of the thermal, stress, and beam propagation modeling that will be presented in this work. Although a number of reports have described kilowatt average power operation of zig-zag slab oscillators using both flashlamp [8], [9] and diode laser pumping [10], residual optical distortions in the solid state gain media have limited the output divergence of these systems to values significantly larger than the diffraction limit. The large one-dimensional temperature gradients through the slab thickness are effectively averaged by the zig-zag optical path but aberrations that result primarily from physical deformations of the slab surfaces in the end face and edge regions remain [7]. For this reason, a useful approach to achieving high average power, high beam quality output from face-pumped, zig-zag slab lasers has included the careful management of the thermally induced slab aberrations as well as the correction of the residual wavefront errors with optical phase conjugation. This can be effectively implemented in a master oscillator, power amplifier (MOPA) pulse extraction geometry incorporating a stimulated Brillouin scattering (SBS) phase conjugate mirror [11].

The SBS phase conjugated MOPA geometry using a face pumped slab amplifier is being actively pursued in parallel with our work and has been successfully implemented by a number of groups [12], [13]. A notable example is the recent report of a high beam quality 100 W average power laser system using a diode laser pumped Nd:YAG slab amplifier that produces 1 J pulses at 100 Hz [14]. This report and the 150 W Nd:glass work presented here represent the highest average brightness measured from solid state laser systems, although the output of the Nd:glass amplifier has a 15× higher peak power as required by applications such as x-ray generation for photolithography.

The high saturation fluence for Nd-doped phosphate glass ($\sim$5 J/cm^2) and the potentially large thermally induced distortions resulting from its low thermal conductivity offer a significant challenge for the operation of a high average power amplifier system. Good thermal management in the form of uniform pumping deposition, uniform cooling, and an optimized amplifier slab design is crucial to successful high power operation. Even under ideal conditions, however, the high fluence required for efficient energy extraction requires carefully designed beam transport and the accurate correction of the remaining thermally induced wavefront aberrations in the amplifier medium in order to avoid damage to optical components. For this reason, the flashlamp pumped Nd:glass amplifier system has been a valuable test bed for the development of high average power solid state amplifier architectures. The result has been robust optical designs which are also read-

Manuscript received June 16, 1993; revised July 8, 1994. This work was supported by the U.S. Department of Energy by Lawrence Livermore National Laboratory under Contract W-7405-Eng-48.

The authors are with the Lawrence Livermore National Laboratory, Livermore, CA 94550 USA.

IEEE Log Number 9407355.

ily applicable to high average power diode-pumped crystalline amplifier systems having lower optical fluences. Numerical codes for thermal analysis, reflector design, energy extraction, SBS phase conjugation, and second harmonic conversion have been experimentally validated and based on these models, a direction for the further scaling of the average power of this Nd:glass amplifier beyond an average power of 500 W has been charted.

There are several key aspects of the design of this amplifier system that have resulted in its successful operation and the achievement of the reported performance characteristics: the choice of an optimized optical extraction architecture, optimized thermal management including the use of specially designed diffuse flashlamp reflectors, and the incorporation of an SBS phase conjugator. In this paper we describe each of these in detail.

II. Optical Architecture

The regenerative amplifier optical configuration is ideally suited to solid state gain media such as Nd:glass. The small stimulated cross section and long spontaneous lifetime (350 μs) give this medium good energy storage characteristics and permit an amplifier system to be operated with many passes and a large system gain without significant losses to amplified spontaneous emission (ASE). The regenerative amplifier effectively provides these gain passes without the complicated optical staging of more conventional MOPA configurations in which extraction beams are angularly multiplexed through amplifier sub-apertures of increasing size.

A. Relay Imaging

Optimal extraction efficiency from a zig-zag slab gain medium requires the amplification of a near top hat spatial beam profile. However, the high aspect ratio rectangular slab aperture combined with this spatial profile results in a beam with poor near field propagation characteristics, particularly in the presence of thermally induced phase aberrations in the solid state amplifier. For this reason, this design uses a 1:1 relay imaging telescope inside of the regenerative amplifier ring which re-images each plane inside the zig-zag slab back onto itself, preserving uniform irradiance spatial profiles in the amplifier for multiple ring passes. A significant part of the design of this system is the use of a double-pass relay telescope as illustrated in Fig. 1. The telescope consists simply of two lenses mounted with an afocal spacing as pressure windows on a vacuum chamber. The counter-propagating beams pass through the lenses offset from the optical axis allowing two separate optical paths through the telescope.

The double-pass telescope geometry offers a number of advantages over a single-pass design. First, it allows the telescope to be constructed with two refractive optics without folding the internal beam paths with reflective mirrors. With only a single pass through a simple two lens telescope, the distance between the conjugate planes would be insufficient to close the regenerative amplifier ring. A more complex multi-element folded relay telescope could be used to extend the distance between the conjugate planes. However, this would require that a number of optical surfaces be located at effectively large propagation distances from the image plane in the laser amplifier. In this case, amplitude modulation due to the propagation of diffraction at the edge of the top hat beam and the propagation of thermal aberrations introduced in the amplifier significantly increases the possibility of damage to optics far from this optical relay plane. A second important advantage of the double passed relay telescope is that it provides an external relay plane on the output of the laser system in which, for example, a frequency doubler can be placed. The same smooth irradiance spatial profile present in the zig-zag slab is relayed into the doubler resulting in uniform second harmonic generation across the output aperture.

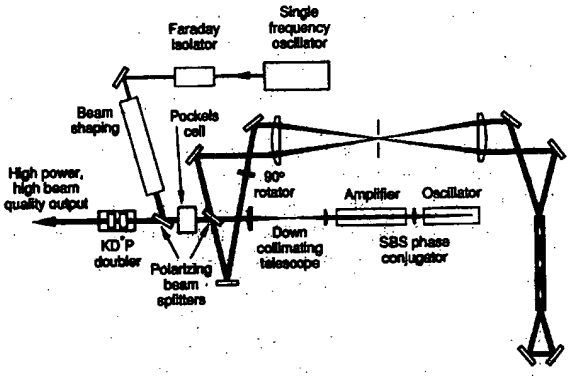

Fig. 1. A schematic diagram of the regenerative amplifier geometry incorporating an SBS phase conjugate mirror. A passive 90° rotator in the regenerative amplifier ring causes the injected pulse to make two ring passes (4 slab passes) before it is directed into the phase conjugator. The SBS wavefront reversed return then retraces the input path for an additional two ring passes, for a total of 8 gain passes, before it exits and is isolated from the input pathway by a Pockels cell. In the original optical layout, without SBS phase conjugation, the Pockels cell was placed inside the ring at the position of the 90° quartz rotator and the output emerged on the beam path that is shown here to enter the SBS cells.

B. Unidirectional Uncorrected Operation

When the laser system is operated as a conventional regenerative amplifier system without SBS phase conjugation, an input pulse from the oscillator enters the system by a reflection off of a polarizing beam splitter placed in the ring as shown in Fig. 1. Although the optical layout shown in Fig. 1 is that for the phase conjugated system, only minor differences exist between the layout for conventional unidirectional operation. The Pockels cell moves from its position in Fig. 1 to a position inside the amplifier optical ring, replacing the 90° quartz rotator. The deuterated potassium diphosphate (KD*P) gas cooled Pockels cell uses 45° quartz rotators as input and output windows so that it also has a passive 90° polarization rotation [15]. Therefore the s-polarized input beam is rotated to p-polarization after passing through the Pockels cell. During the first ring revolution, the half wave ($\lambda/2$) voltage is applied to the Pockels cell crystals so that further polarization rotation is prevented and the input pulse is trapped in the regenerative amplifier ring until the voltage is removed. In this zig-zag amplifier design, near normal input and output faces are used

on the glass slab with sol-gel antireflection (AR) coatings [16]. This allows the slab to be double passed in a "diamond" pattern as shown in Fig. 1 and either s or p-polarized beams can be amplified. When the Pockels cell voltage is switched back to zero, the injected pulse makes one more ring pass in s-polarization, corresponding to two more gain passes. The Pockels cell is therefore not required to transmit the fully amplified output pulse energy, reducing the possibility of optical damage to the KD*P. The amplified output pulse exits the system along the beam line that is shown in Fig. 1 to lead to the SBS phase conjugator.

It is necessary to add a baffle plate at the center of the relay telescope to serve as a field stop. During the 200 μs flashlamp pulse, prior to injection of the oscillator extraction pulse, the 90° rotation of the passive Pockels cell prevents parasitic oscillation in the regenerative amplifier ring by providing a >99% loss at the polarizing beam splitter on every other ring pass. However, for incident angles on the quartz rotator crystals larger than ~15 mrad, the amount of polarization rotation is insufficient to prevent oscillation. A 10 mm field stop placed at the focus of the 120 cm telescope lenses prevents angles larger than ~4 mrad to be relayed in the amplifier ring and suppresses this source of parasitic oscillation.

C. Operation With an SBS Conjugator

By replacing the Pockels cell in the regenerative amplifier ring with a 90° quartz rotator as depicted in Fig. 1, an injected pulse from the oscillator makes two revolutions through the ring, for a total of four gain passes, before it is reflected by the polarizing beam splitter. This reflected beam, formerly the output beam in the uni-directional configuration, is now directed into an SBS phase conjugation cell. The wavefront reversed return from the conjugator retraces the two ring passes, accumulating four more gain passes, before it is again reflected out of the ring. The high power pulse is now retracing the input beam path and must be isolated from the oscillator. This is accomplished by placing the Pockels cell removed from the ring into the input beam as illustrated in Fig. 1. The $\lambda/2$ voltage is applied to the Pockels cell as the injected seed pulse is transmitted into the ring, canceling its passive 90° rotation. During the following four ring transit times, the Pockels cell voltage is switched back to zero so that the high energy output pulse experiences a 90° rotation and is transmitted through the input polarizing beam splitter.

The most important advantage of operating the regenerative amplifier system with an SBS mirror lies, of course, in its wavefront reversal properties. As the input beam makes its first four passes through the amplifier, it accumulates wavefront phase errors due to thermal aberrations in the solid-state slab as well as to residual optical figure errors in the other optics in the ring. The SBS cell effectively conjugates the phase of the input beam producing a wavefront reversed output Stokes beam with only a small frequency shift (~5 GHz). As this output beam retraces the path of the input beam through four additional gain passes, the phase errors cancel and the high quality wavefront of the injected beam is recovered in the high energy output.

There are additional significant advantages to the operation of the amplifier system with the SBS phase conjugator. Eight gain passes through the zig-zag slab amplifier can be achieved using passive polarization switching in the regenerative amplifier ring. The fact that the SBS cell provides interstage gain isolation makes this possible since, if it were replaced with a mirror, the small signal gain through eight consecutive gain passes would result in possible parasitic oscillation from the small reflective losses of AR coated optical surfaces in the ring or in the output beam. When the Pockels cell is located inside the regenerative amplifier ring, the length of the laser pulse to be amplified is limited to the transit time inside the ring minus the high voltage switching time for the Pockels cell. Now, with passive polarization switching, this time limit is increased to be the transit time for four ring revolutions. Longer pulses can be amplified and the relative timing accuracy requirement between the injected pulse and the Pockels cell voltage pulse is greatly reduced. In fact, the replacement of the Pockels cell with a full aperture Faraday isolator has been shown to allow the amplification of laser pulses of up to 500 ns in duration [17].

The SBS phase conjugator very effectively conjugates the first order aberration of tilt. This greatly reduces the sensitivity of the system performance to small changes of optical alignment in the ring. No change in output power or pointing direction during operation are observed for large mirror misalignments in the ring, limited only to those angular excursions that result in vignetting of the beams at the edges of the amplifier slab.

D. Single Frequency Oscillator

The 1053 nm transition in Nd:YLF closely matches the fluorescence curve peak in the Nd doped phosphate glass used in this amplifier system. It is desirable to have a single frequency oscillator input pulse both for generating reproducible smooth temporal input profiles without modulation from multi-longitudinal modes and for achieving the best wavefront reversal fidelity in the SBS phase conjugator [19], [18]. Although single longitudinal mode output from a Nd:YLF Q-switched oscillator has been demonstrated by injection locking to a low power single frequency master oscillator, this technique requires careful mode matching between the master and slave oscillators and active cavity length stabilization of the Q-switched slave oscillator [20]. A simpler method of achieving single frequency output was chosen for this application by using a variation of the electronic linewidth narrowing technique [21], [22]. In this method, very low power oscillation is allowed to build up in the Q-switched cavity over an extended period of time (1–2 μs). By placing a frequency selective element such as an etalon in the cavity, this long build up time and the corresponding many passes through the etalon results in single longitudinal mode oscillation. The intracavity power is monitored by the leakage through the high reflectivity (HR) mirror and when it peaks in a weak relaxation oscillation, the Q-switch is opened. The low power single frequency flux then serves to seed the build up of a high power Q-switched pulse.

A thin film polarizing beam splitter in combination with a $\lambda/4$ waveplate is used to prevent laser oscillation during the flashlamp pumping pulse. By slightly rotating the $\lambda/4$ waveplate from the position of maximum extinction, the cavity is allowed to leak in order for the weak single frequency self seeding power to build up. A 30-mm solid fused silica etalon with 40% reflective coatings is used as a frequency selective optic. By varying the gain in the Nd:YLF rod at the time of Q-switching, pulse widths between 8 and 25 ns are achievable with 40 to 5 mJ output energy per pulse, respectively. The oscillator is generally operated at 13–14 ns full width half maximum (FWHM) with 25 mJ per pulse. Although longitudinal mode hopping is observed from one output pulse to the next over a period of operation, each individual output pulse is always reliably single frequency. No closed loop cavity length stabilization is required.

The output of the single frequency Nd:YLF Q-switched oscillator is amplified to ~100 mJ using additional Nd:YLF pre-amplification. The beam is then anamorphically expanded to match the aspect ratio of the extracted aperture of the zig-zag slab. A slightly oversized elliptical beam is clipped by a hard rectangular aperture and relayed to a point conjugate to an image plane in the slab as depicted in Fig. 1. In order to efficiently extract the stored energy in the slab amplifier in 8 gain passes, an injected seed energy of 60 mJ is required as will be described in greater detail in Section V.

III. Amplifier Design

The goal of the amplifier design is to maximize the efficiency and uniformity of the upper laser level activation in the gain medium while minimizing thermally induced distortion and depolarization of the transmitted optical wavefront. The major components of the amplifier design are the zig-zag slab, the cooling system, and the flashlamp and reflector assemblies. The choice of a slab geometry requires analyses of the gain and energy storage required for the desired output energy, the ASE energy storage losses, and the thermally induced optical aberration and depolarization.

A. Amplifier Slab

The amplifier slab design for this regenerative amplifier system is illustrated in Fig. 2. The zig-zag slab is 1 cm wide, 14 cm tall, and 40 cm long for a total volume of 0.56 l. It is composed of the neodymium (Nd) doped phosphate glass APG1 supplied by Schott Glass Technologies Inc. or HAP4 supplied by Hoya Corporation. The Nd doping level in both cases is 3×10^{20} cm^{-3} or 2.7% by weight. The laser beam enters the slab 13° from the long slab axis so that it is reflected three times from each side of the slab, for a total of six bounces, before exiting the other end. This pathway, combined with the counter-propagating second path, provides nearly complete optical fill and forms a six diamond pattern through the amplifier. Fig. 1 illustrates only three diamonds for clarity.

To minimize the possibility of internal parasitic oscillation, 2 mm thick copper doped absorbing glass is attached to the top and bottom edges of the glass amplifier slab using an index of refraction matching elastomer, as illustrated in Fig. 2. In addition, the input and output faces are parallel, but oriented 1.5° from normal so that a ray perpendicular to one face cannot intersect the opposite face. Numerical modeling indicates that a larger wedge angle on the slab end faces could further decrease stored energy losses due to ASE and allow an even higher maximum gain coefficient to be achieved. However, the use of indexed matched edge cladding with this near square ended slab geometry easily results in the required stored energy to efficiently extract a 25 J laser pulse. Experimental measurements of energy storage in this amplifier are presented in Section V.

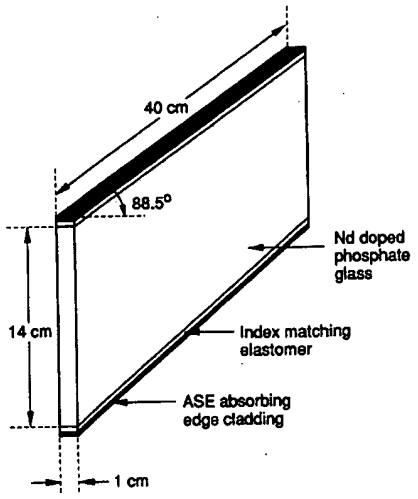

Fig. 2. The Nd:glass slab design used in this amplifier system. The input and output faces are parallel and are oriented 1.5° from normal. An ASE absorbing edge cladding is attached to the top and bottom edges of the slab using an index matching polyurethane elastomer.

B. Amplifier Cooling and Thermal Analysis

The laser amplifier was designed using a three dimensional code which, given the material constants, slab geometry, and thermomechanical boundary conditions, numerically solves for the temperature, stress, and deformation distributions within the slab.[1] Zig-zag path optical rays are then traced through the thermally loaded medium resulting in a map of wavefront distortion and depolarization for the amplifier aperture [7]. The goal in the amplifier design is to combine a set of material properties with a geometrical configuration that minimizes optical beam aberrations. Since the transmitted beam quality is dependent on the spatial distribution of thermal sources and sinks and on thermomechanical boundary conditions, the edges are particularly sensitive and must be treated with care.

[1]The computer code TECATE numerically solves for the temperature, stress, and deformation distributions and BREW calculates the transmitted optical wavefront. These codes were originally developed for use in the ICF program by LLNL scientists R. J. Gelinas and S. K. Doss. Time dependence in the thermal computations and a generalized surface source simulating lamp or diode laser pumping were later implemented in TECATE by S. K. Doss, J. A. Blink, and L. E. Zapata to accommodate zig-zag amplifiers such as this one.

Using these codes, the effects of design parameters such as optical pump distribution, cooling conditions, and fluid seal locations can be investigated by numerical experiments. When an optimal design is found, the hardware is then configured to achieve the conditions prescribed by the codes as nearly as possible.

One-dimensional pumping nonuniformities in the propagation dimension are averaged effectively by the zig-zag pathway of the beam provided that they have low spatial frequency compared to the size of the beam footprint projected onto the pump faces. Sensitivity studies reveal, however, that even a gently rolling variation in pumping uniformity across the 14 cm vertical slab dimension with a 5% deviation from the average translates into a single pass wavefront error of about one wave. Sharper two dimensional variations have been modeled and the results depend on the size, location, and the depth of the modulation. It was found that hot spots of 5 cm diameter and approximately 5% above the average pumping irradiance can introduce 2–3 λ of distortion into both the horizontal and vertical dimensions of the beam and also generate local depolarization losses of a few percent. The next order of design sensitivity lies in the design of the slab cooling fluid channel seal made at the slab ends normal to the 40 cm dimension. This seal and associated hardware necessarily project a shadow onto the end of the active medium. Calculations indicate that for this slab geometry no more than 5 mm of the ends should be shaded in order to avoid significant wavefront error and depolarization.

For the required average laser amplifier output power, the design point for the slab was set at 1 W/cm^3 of heat, resulting in a surface heat flux of 0.5 W/cm^2. The removal of waste heat from the laser slab is accomplished by water cooling of the large pump surfaces. Turbulent water flow maximizes heat transfer and the resulting high flow rate minimizes the temperature rise in the flow direction. A surface convection coefficient in the neighborhood of 1 to 4 W/cm^2/K is typical although the exact value of this parameter does not strongly impact the modeling predictions. Wavefront distortions add less than a quarter wave in the narrow dimension when the film coefficient is allowed to vary by a factor of 4 along the long dimension of the slab. In the other dimension, a small wedge angle is imposed on the beam due to the water temperature rise and amounts to approximately three waves of tilt per °C temperature rise. At the flow rates used here, a measured temperature rise of 0.1°C was found to correlate well with interferometric data and is consistent with the removal of 500 watts of heat from the surfaces of the slab.

Fig. 3 is an experimentally measured interferogram of the amplifier slab used in this work. The probe beam made two passes through the amplifier and the slab was thermally loaded at 7.5 kW average lamp power, the operating point for 75–90 W average laser output power. The measurements show a peak-to-valley single pass distortion of ~1λ in the vertical dimension and 0.05λ in the horizontal dimension of the extraction aperture. Fig. 4 shows the computed interferogram and depolarization contours which compare well with the measurements both in qualitative shape and in overall magnitude. These measurements and calculations illustrate

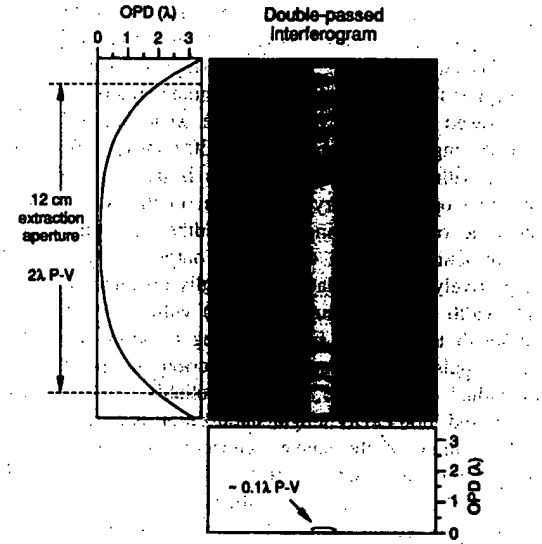

Fig. 3. A double passed 1 μm interferogram of the amplifier slab with 2500 J flashlamp energy at 3 Hz PRF. The peak to valley single pass distortion is 0.05λ and 1λ in the extracted horizontal and vertical dimensions, respectively.

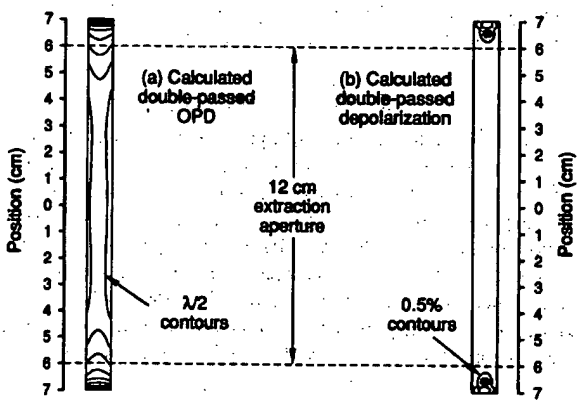

Fig. 4. The numerically predicted double pass optical distortion and depolarization for the same operating conditions of Fig. 3. The extraction beam through the 14 cm slab is limited to 12 cm to avoid the regions of peak depolarization at the top and bottom of the slab. The experimentally measured optical distortion shown in Fig. 3 is in reasonable agreement with this calculated performance.

both the predictive power of the modeling and codes and the successful design and engineering that met the required operating conditions prescribed by these codes.

C. Diffuse Reflector Design

The goal of the flashlamp and reflector assembly design is to produce a homogeneous pumping profile in the gain medium with high efficiency. As described in the previous section, a uniform pump irradiance profile across the pump faces of the slab is required to produce minimum thermal aberrations. Although the zig-zag path through the slab effectively averages one-dimensional index gradients through the thickness of the slab, any nonuniformities in the vertical dimension are directly

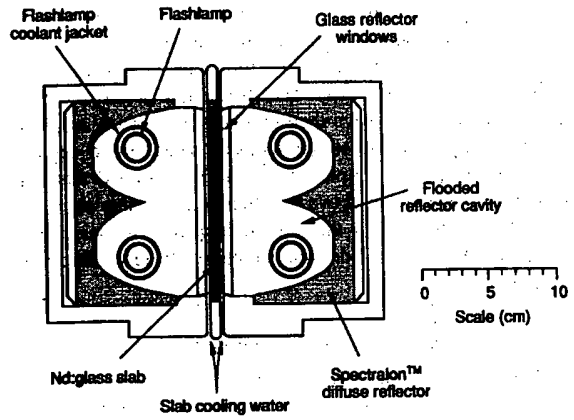

Fig. 5. A schematic illustration of the amplifier head design. The diffuse flashlamp reflectors are shaped from solid pieces of Spectralon™ and the Nd:glass slab is cooled by 3 l/s water flow through 2.5 mm channels on each side of the slab.

imposed as aberrations on the transmitted beam. Even under perfectly uniform pumping conditions, stress discontinuity and geometrical pump fall off phenomena near the edges generate depolarization and wavefront errors. These typically invade a portion of the top and bottom of the amplifier aperture equal to one slab thickness. This could be compensated by a specific nonuniform intensity profile near the edges but this would require a more complex reflector design, probably involving both diffuse and specular components. Instead, it was chosen to limit the extraction aperture in the 14 cm tall slab to 12 cm.

In order to achieve the required high degree of pumping uniformity and good transport efficiency, the flashlamp reflectors were machined from solid blocks of Spectralon™. The material has very high reflectivity (>99%) across the visible spectrum and when used in a water flooded reflector enclosure, exhibits a very high damage threshold. With an incident flashlamp fluence of 2.5 J/cm^2, no degradation has been observed for >5 million flashlamp pulses.

The reflectors are machined to a specific shape as illustrated in Fig. 5 to tailor the pumping irradiance distribution on the surfaces of the amplifier slab. In order to design the reflectors, a two-dimensional ray trace code has been developed. The analysis models the emission from the lamps, the reflection from the reflector surfaces, the absorption and transmission through the slab, and the reabsorption and reemission by the flashlamps. The calculation is performed in the two dimensions normal to the length of the flashlamps. The emission from a flashlamp is assumed uniform over its surface (in this plane a circle) with a cosine squared angular distribution relative to the local surface normal to the lamp. This distribution arises by treating the lamps as black bodies and has been found to be in good qualitative agreement with experimental observations. This black body assumption will be addressed further in the following discussion.

After a ray is emitted from a lamp it propagates until hitting a surface. If the surface is a reflector segment, it is reflected with a specified energy reflectance either in a specular or diffuse manner, depending on the reflector construction material. For a specular surface, the ray simply reflects about the normal to the segment. The diffuse reflection is modeled by a perfectly Lambertian surface with the reflected ray being weighted by a cosine distribution. Rather than generating a fan of new rays at every reflector intersection, a single randomly generated ray is traced. This new randomly oriented ray is appropriately weighted and normalized such that energy is conserved for an ensemble of rays. This treatment is valid provided a sufficiently large number of rays are tracked through the reflector.

An average absorption coefficient is used for the glass slab generated by convolving the flashlamp emission spectrum with the slab absorption spectrum. The rays which strike the slab are attenuated based on this coefficient and then treated as if they encountered a specular reflector segment. This assumes symmetric pumping from both sides of the slab which is typical for single slab geometries such as this one. The absorbed energy is accumulated as function of slab position in order to predict the pumping distribution across the gain volume.

If a ray intersects a lamp it is absorbed and terminated. Because some fraction of the rays intersecting the lamp will transmit and some portion will serve to repump the lamp plasma, a reemission coefficient is specified which keeps track of what fraction of the absorbed energy would normally by recycled into the spectral pump band of interest. This reemission factor has no effect on the spatial distribution since it assumes the majority of the recycled energy will be uniformly emitted at the lamp surface, just as for the original rays. For lamps excited at a relatively low current level, this will introduce a larger error than for lamps driven at a significant fraction of the explosion limit, giving their emission a spectral distribution more characteristic of a black body. Treating the lamps as black rather than gray bodies has the effect for specular reflectors to sharpen the images of the lamps generated on the slab. In the case of diffuse reflectors, this effect can be neglected. Each individual ray is tracked from its origin at the lamp until it has lost a specified fraction of its starting energy.

Fig. 6 illustrates the predicted performance (open circles) of the diffuse flashlamp reflectors designed with the aid of the described code for the present Nd:glass zig-zag amplifier. Also displayed (solid curve) is a line out of the experimentally observed fluorescence imaged at the exit aperture of the slab through a 1-mrad field stop. As can be seen, good energy deposition uniformity is achieved along the face of the slab and this performance was accurately predicted by the flashlamp reflector design code. The degree of pumping uniformity in the extracted amplifier aperture was increased by a factor of ten over that of previous specular reflector designs used in this system.

IV. SBS Phase Conjugation

The basic concept of SBS phase conjugation is well understood and widely documented in the literature [23]. However, there are a number of important considerations to be made when incorporating an SBS phase conjugate mirror into a high

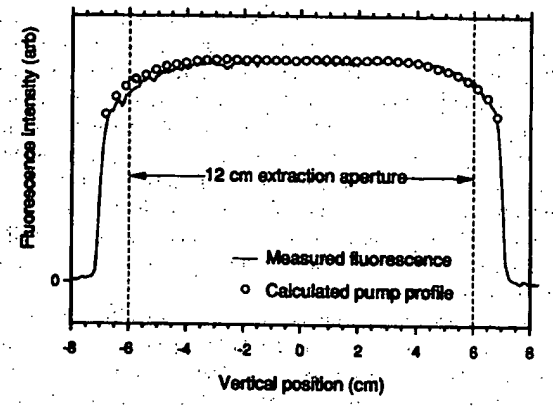

Fig. 6. A comparison of the numerically predicted (○) and experimentally measured (solid curve) pumping uniformity. The measurement was made by imaging the fluorescence at the output aperture of the slab through a 1 mrad field stop.

power laser system in order to accommodate the often required high input energies and to maintain good near and far field fidelity in the output.

A. Wavefront Reversal Fidelity

It has been proposed that for optimal wavefront reversal fidelity, the SBS phase conjugator should not be operated more than five times above the threshold of stimulated Brillouin return [24]. In that report, large shot to shot fluctuations in the wavefront of the Stokes output were measured when the SBS threshold was greatly exceeded. However, we have recently demonstrated that this observation was related to the slope of the rising edge of the input laser pulse relative to the acoustic decay time (τ_B) in the Brillouin medium [25], [26]. It was shown that the results of [24] using high pressure nitrogen gas could be reproduced by placing a very fast leading edge on the input pulse. Of more importance, however, it was also shown that these fluctuations could be reduced by tailoring the risetime of the leading edge of the pulse such that it was longer than τ_B for the SBS material. Using carbon tetrachloride (CCl_4) with $\tau_B \sim$ 1-ns and 13-ns FWHM input pulses with near Gaussian temporal profiles, good shot to shot fidelity was demonstrated at over 100 times above threshold. These observations were also confirmed in measurements by other researchers in which good wavefront reversal fidelity was demonstrated at up to 50 times threshold using Freon-113 [27]. They also observed fidelity degradation with high pressure nitrogen but attributed it, we believe incorrectly, to competition from stimulated Raman scattering or nonlinear self focusing.

The conclusion that good wavefront reversal fidelity in the SBS Stokes waves is obtainable for input powers high above threshold is very significant given that there are strong motivations for operating the SBS phase conjugator with large input energies. In a simplified understanding of the SBS phase conjugation process, an input wave with a uniform irradiance spatial profile and flat phase profile is transmitted through an aberrating medium. If this beam is then focused into an SBS cell, the aberrated wavefront is transformed into a distorted irradiance spatial profile in the far field. The Stokes wave is seeded from random acoustic fluctuations in the medium and is selectively amplified by stimulated scattering in the regions of peak irradiance. The diffraction of the resulting counter propagating wave then produces a reversed, or phase conjugated, wavefront at the focusing lens. Based on this description, albeit a simple one, it can be reasoned that it is desirable to operate far above threshold with a highly aberrated input beam in order for the highest frequency modes, which often appear as small side lobe structures, to reach threshold and be reversed.

B. SBS Amplifier/Oscillator Configuration

In general, the limit to the peak power that can be delivered to a focused SBS phase conjugate mirror is determined by competing processes such as stimulated Raman scattering, self focusing, and optical breakdown. This limitation can be overcome by using a two cell system configured in an oscillator/amplifier arrangement [28]. As depicted in the optical layout of Fig. 1, the collimated input beam is directed through the first SBS cell and then focused into a second cell. In this way the peak optical power in the focused oscillator cell is reduced by the SBS amplification of the Stokes wave in the collimated amplifier cell. The beam cross section in the collimated cell is nominally adjusted such that the peak gain, irradiance, and length product (gIL) is ~30, near the threshold for stimulated return from that cell alone. In practice, however, it is found that very efficient amplification in the first cell is achieved with a calculated peak gIL product of ~45. Even at this large value, no spontaneous SBS contribution is observed from the amplifier cell since saturation of the incoming laser pump pulse prevents the gain product from reaching the estimated value.

Another consideration in configuring the SBS oscillator/amplifier system is the round trip optical propagation length in the SBS medium. This should not greatly exceed τB for the SBS material. In this case, when the SBS system is driven high above threshold, strong pulse reshaping in the Stokes return in the form of pulse compression can result. For input pulses of sufficient duration, periodic modulation with a period corresponding to the round trip time through the SBS cells is observed. In this amplifier system, the input beam was configured with a cross section of ~1 cm^2 (8 × 12 mm^2) through a 33 cm amplifier cell. It was then focused into the oscillator cell with a 14 cm focal length lens. Although saturation in the amplifier cell allows attenuation to be added in front of the oscillator cell without a great penalty in energy efficiency, it was not found to be necessary up to an input energy of 3 J in a pulse width of 13 ns.

C. Relay Imaging to the SBS Cell

A highly relayed optical system, as described in previous sections, is essential for the successful operation of a phase conjugated amplifier system. As wavefront aberration accumulates on the laser pulse circulating in the amplifier, the system optics must collect, relay, and deliver to the SBS cells all components of the aberrated beam. In addition to this, we have

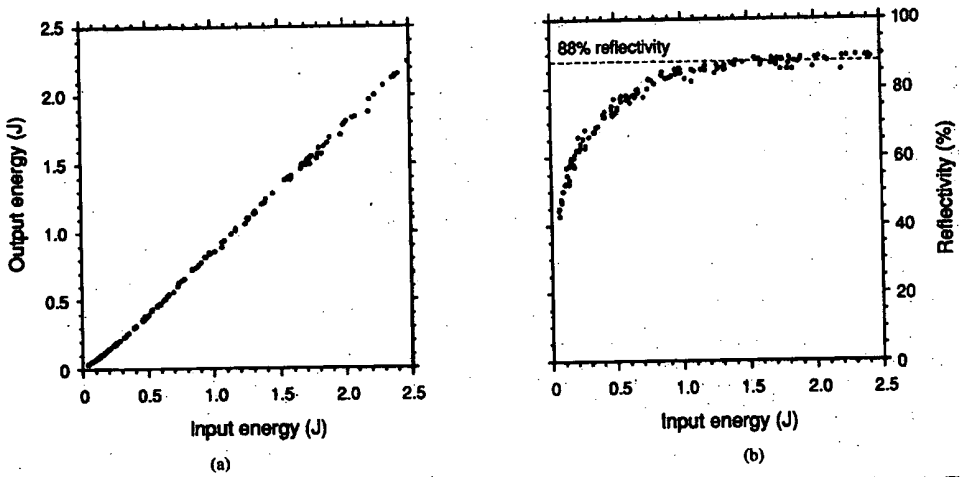

Fig. 7. (a) The experimentally measured reflected energy versus input energy for the two cell SBS phase conjugator arrangement. (b) The same data plotted as SBS reflectivity versus input energy.

found that the irradiance spatial profile delivered to the SBS oscillator is also significant. It is important that aberrations on the wavefront not be allowed to free propagate, producing a distorted irradiance spatial profile. The near field reproduction in the SBS conjugator return is observed to be poor for a strongly modulated input irradiance profile. If the distorted phase information is lost to near field distortion in the beam, then this poor near field reproduction will degrade the phase conjugation fidelity of the SBS mirror. By image relaying the amplifier aperture to the focusing lens of the SBS oscillator, a smooth spatial profile is presented to the phase conjugator. Any errors in the near field irradiance distribution in the SBS return in the form of small amplitude modulation are then corrected by gain saturation in the final amplifier passes.

D. Temporal Fidelity

It is also important to operate the SBS phase conjugator high above threshold to have high reflectivity and the best reproduction of the temporal profile of the input pulse. The energy efficiency of the phase conjugate mirror is determined primarily by the leading edge portion of the input pulse that is transmitted through the cells and lost before the SBS threshold is reached. For this reason, maximizing the SBS efficiency also optimizes the temporal reproduction fidelity of the input pulse. Fig. 7 shows the reflectivity vs. input energy for the described two cell amplifier/oscillator configuration up to the nominal operating input level of 2.5 J. The reflectivity saturates at a maximum value of 88% beyond ~1 J. The insertion loss into the amplifier is very small with this high value of the SBS conversion efficiency and virtually no pulse shortening or steepening of the leading edge of the output temporal profile is observed.

E. SBS Medium Purity

The purity of the SBS medium is very important with respect to minimizing both optical absorption and the possibility of optical breakdown at the focus of the SBS oscillator. The removal of dissolved impurities which can undesirably increase absorption can normally be accomplished by distillation techniques. In practice, however, we have determined that in the case of CCl_4, it is sufficient to use the commercially available 99.9% spectroscopic grade liquid. However, a more challenging problem was found to be the presence of suspended particulate impurities which, when intercepted by the focused input beam, lead to a significantly reduced optical breakdown threshold. The most effective way of removal of these particles has been found to be the use of a closed loop filtration system installed on the SBS oscillator cell. A small centrifugal pump of stainless steel and teflon construction is used to circulate the CCl_4 through a 0.1-μm filter. Once the cell has been adequately filtered, it is not necessary to operate the circulation system during operation of the laser amplifier. After filtration, the optical breakdown threshold for the 10–15 ns input pulses is increased from 40 mJ to over 1 J for the single cell focused SBS oscillator.

V. Energy Storage and Extraction Efficiency

The Nd:glass slab is pumped by four 170 torr Xe flashlamps with an inner bore diameter of 18 mm and an arc length of 39 cm. The lamps are excited with a critically damped current pulse with a full width of 270 μs measured at 10% of peak. Fig. 8 shows experimental gain measurements versus electrical energy deposited in the flashlamps. A single pass small signal amplification of 6.2 is demonstrated with 4.1 kJ of lamp energy, the maximum energy available from the configuration of the flashlamp electrical pulser. As illustrated in Fig. 8, when this same data is plotted as stored laser energy density, a linear relationship is observed without significant roll off due to losses by ASE.

Although the data of Fig. 8 show a potential total stored energy of 120 J in the laser slab, the maximum energy extracted from the amplifier in a 13–14 ns laser pulse is limited to 30 J due to the possibility of nonlinear self focusing in the amplifier glass. Even for this pulse energy, the amplifier cannot be operated in a highly saturated extraction regime. The increased glass propagation distance at high irradiance

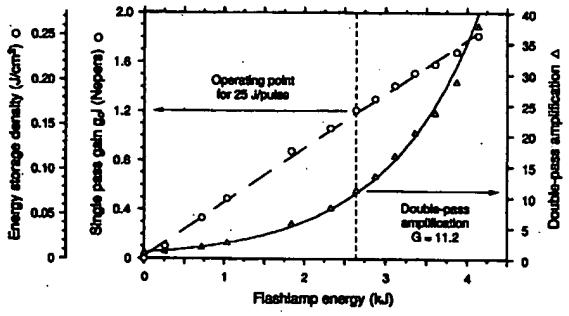

Fig. 8. The experimentally measured single pass gain (○) and double pass small signal amplification factor (△) versus flashlamp energy. The slope of the single pass gain curve corresponds to a energy storage efficiency of 3% and remains linear over the available flashlamp energy range without significant roll-over due to ASE losses.

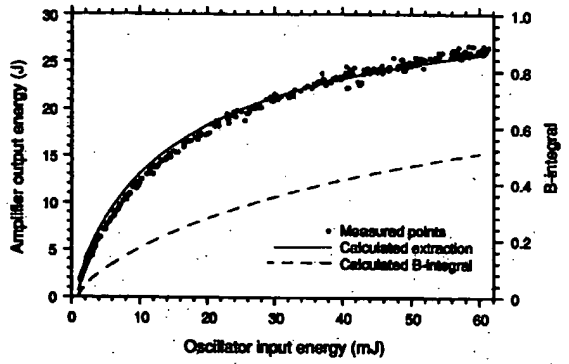

Fig. 9. The experimentally measured amplified output energy versus input energy from the oscillator for 2500-J flashlamp energy and a single pass small signal amplification of ~3.5. The solid line is the numerically predicted extraction curve calculated using a Frantz–Nodvik model. The dashed line is the accumulated B-integral calculated over this output pulse energy range.

required to achieve very large extraction efficiencies can result in beam filamentation and bulk glass damage. For this reason, an optimal operating regime for 25 J output results from storing 75 J in the amplifier slab with a single pass amplification ratio of 3 and an optical extraction efficiency of ~33%. As illustrated in Fig. 9, 25 J can be extracted in a 14 ns pulse with an oscillator input energy of 60 mJ. This results in an input energy of ~2.5 J to the SBS cells. The B-integral, a scaled product of the nonlinear index and optical irradiance integrated over the propagation distance, reaches a value of ~0.5. This is a factor of 5–6 below the expected onset level of self-focusing for a beam with a smooth irradiance profile [29]. Also plotted in Fig. 9 is a theoretically calculated energy extraction curve using a Frantz–Nodvik numerical model [30]. When the SBS phase conjugator reflectivity curve of Fig. 7 and an experimentally measured regenerative amplifier ring transmission of 90% are included in the model, good agreement is observed between the predicted and measured output energies.

VI. Output Beam Quality

In order to extract high beam quality output from the phase conjugated amplifier system, a high quality input pulse must be

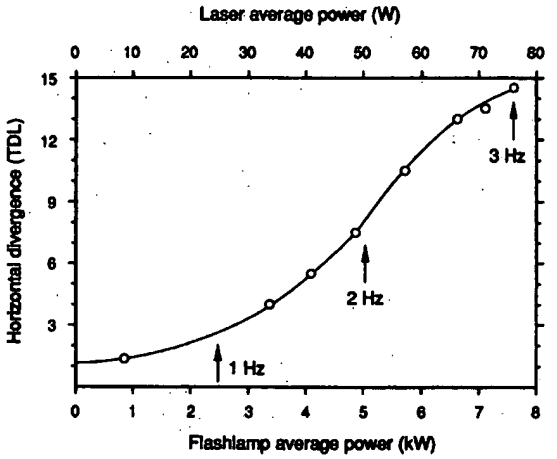

Fig. 10. The measured output divergence in the narrow beam dimension vs. repetition rate for 25 J output pulses. At 3 Hz, with an average flashlamp power of 7.5 kW, the divergence is increased to almost 15× the diffraction limit.

provided. In ideal operation, the wavefront reversal achieved in the SBS phase conjugator allows the spatial phase distribution of the input beam to be reproduced in the amplified output beam. Using the previously described single frequency self-seeded Nd:YLF oscillator, excellent seed beam quality has been measured with less than 1.1× the diffraction limited divergence. The 25 mJ output of this oscillator, however, must be further amplified and anamorphically expanded to provide the ~60 mJ, 8 × 120 mm input to the amplifier system. The divergence of this injected pulse is increased to 1.25× the diffraction limit in this process, primarily due to optical aberrations in the Nd:YLF preamplifier.

As the pulse repetition frequency of the laser system is increased, the thermal aberrations shown in Fig. 3 result in significantly increased output divergence when the amplifier is operated in the unidirectional uncorrected mode without the SBS phase conjugate mirror. The measured output divergence vs. repetition rate is shown in Fig. 10 for 25 J output pulses. At 3 Hz with an average output power of 75 W the divergence in the narrow beam dimension is increased to almost 15× the diffraction limit. However, when the amplifier system is configured as described previously with an SBS phase conjugator, the divergence does not measurably increase up to the maximum achievable pulse repetition frequency. Fig. 11 compares the corrected and uncorrected far field profiles measured at the focus of a 120 cm corrected aspherical lens for 3 Hz, 75 W operation. With the phase conjugator, the width of the far field pattern is dramatically reduced to a single central peak with small side lobes characteristic of the angular distribution from a near uniformly filled aperture.

The 8 × 120-mm output of the amplifier system is characterized by smooth reproducible beam profiles. Fig. 12 shows (a) a CCD image of the near field output imaged at the external relay plane conjugate to the amplifier aperture and (d) the far field recorded at the focus of a lens. In order to quantitatively evaluate the measured divergence of the amplifier output, the

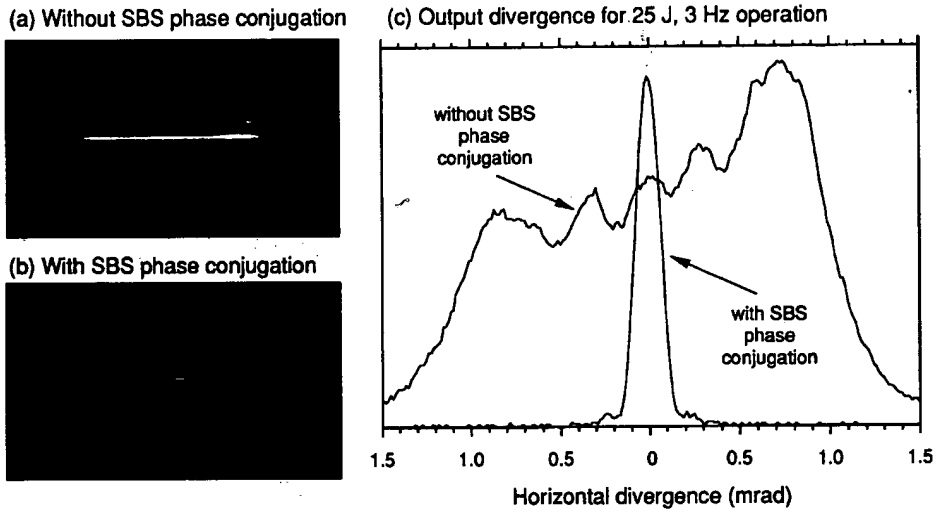

Fig. 11. A comparison of the far field profiles measured at the focus of a 120 cm lens for 3 Hz, 75 W operation (a) without and (b) with SBS phase conjugation. Plot (c) overlays horizontal cross-sections of both cases.

theoretically expected diffraction limited divergence of a beam having the observed irradiance spatial distribution must be determined. A two-dimensional super-Gaussian distribution is first fitted to the near field profile. A comparison of this fit to cross sections of the measured profile is shown in Fig. 12 (b), (c). The results of this numerical fit is then Fourier transformed to generate an expected far field distribution given a perfectly uniform phase profile. Fig. 12 (e), (f) plots the predicted and experimentally measured far field patterns for the horizontal and vertical dimensions. It is found that if the divergence scale for the measured data is reduced by a factor of 1.25, nearly exact overlap of the calculated and measured profiles results. It is significant to note that this is the same divergence measured for the input pulse to the amplifier as illustrated by the overlay of the far field profiles of the input and amplified output beams in Fig. 13 (a). It is concluded therefore that the beam quality of the high power output is presently limited by that of the low power input.

The results of the analysis of the far field images indicate that there is a far field output lobe whose width is 1.25× that expected for a diffraction limited beam. However, it is important to determine what fraction of the measured output energy is contained in this narrow peak. There is the need to rule out the possibility that high spatial frequency irradiance or phase modulation is scattering a significant but undetected portion of the radiation into larger divergence angles. The dynamic range of the CCD cameras is such that a very low irradiance distributed evenly across the image background could fall below the signal-to-noise detection limit of the camera but still account for a significant fraction of the total output power. A straightforward measurement that can be made in this regard is the transmission of an aperture placed at the focus of the analysis lens. In this case an aperture was chosen that was 0.5 mm in diameter corresponding approximately to the distance between the first minima in the horizontal dimension of the measured far field profile. The expected transmission of this "bucket" for a 1.25× diffraction limited beam is calculated to be 96%. As illustrated in Fig. 13(b), a transmission of ~92% was measured across the range of output energies up to 25 J. This 5% reduction in the expected transmission is reasonable based on the fact that the fit between the super-Gaussian and measured near field profiles shown in Fig. 12(b), (c) is not perfect. The small scale irradiance modulation on the beam profile is expected to contribute to a small reduction in Strehl, as was observed in the measurements.

VII. Average Power Operation

In the present configuration of this flashlamp pumped Nd:glass amplifier system, the lamps can be pulsed at repetition rates of up to 6 Hz with 2.5 kJ deposited electrical energy per pulse before reaching the stress fracture limit of the amplifier glass. When the laser amplifier system is operated in the SBS phase conjugated configuration, the near field irradiance distribution and far field divergence described in the previous section is maintained up to this full pulse repetition frequency. In fact, in an experiment in which the amplifier slab was intentionally thermally loaded above 6 Hz, near diffraction limited output divergence was preserved up to the last laser pulses before the slab fractured. The amplifier system has been operated for periods exceeding 1 hr with average output power above 150 W. Fig. 14 illustrates continuous records of laser pulse energies between 25 and 27 J for 4-, 5-, and 6-Hz operation. The temporal profile of the amplified output pulses is characterized by a smooth, unmodulated envelope without a steep leading edge that would be characteristic of significant temporal reshaping in the phase conjugator. The plot of a single temporal waveform as well as that of ~1800 superimposed waveforms collected at 4 Hz are shown in Fig. 15.

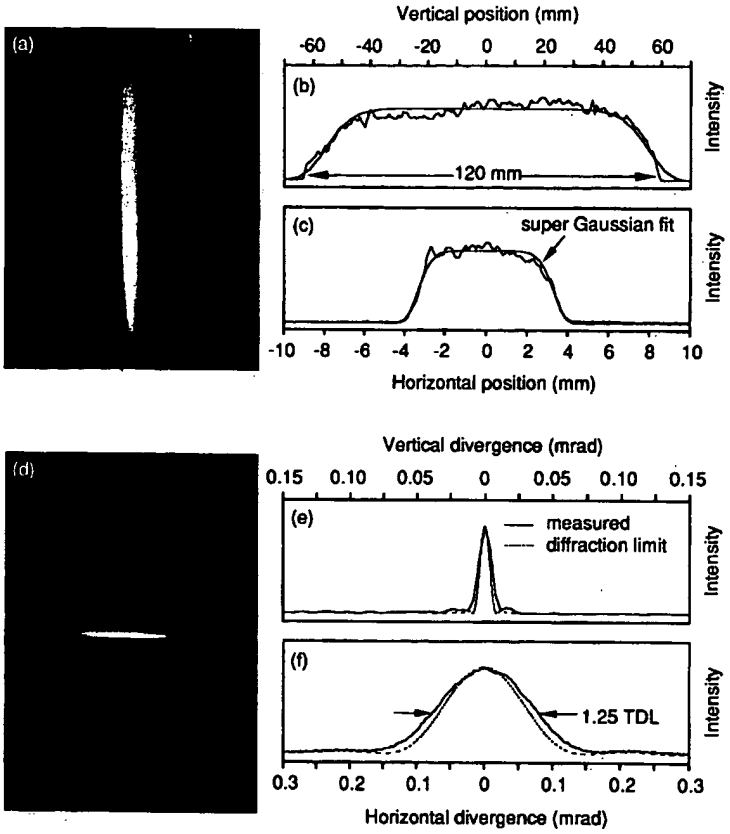

Fig. 12. (a) CCD image of the near field output imaged at the external relay plane conjugate to the amplifier aperture. (b) and (c) show vertical and horizontal cross sections of this profile, respectively. The smooth curve plotted with each cross section is the result of a super Gaussian fit to this near field profile. (d) CCD image of the far field profile measured simultaneously with the near field profile. A comparison between (e) vertical and (f) horizontal cross sections of this profile and the Fourier transform of the super Gaussian fit of the near field profile is shown. It is found that if the divergence scale for the measured data is reduced by a factor of 1.25, nearly exact overlap of the calculated and measured profiles results.

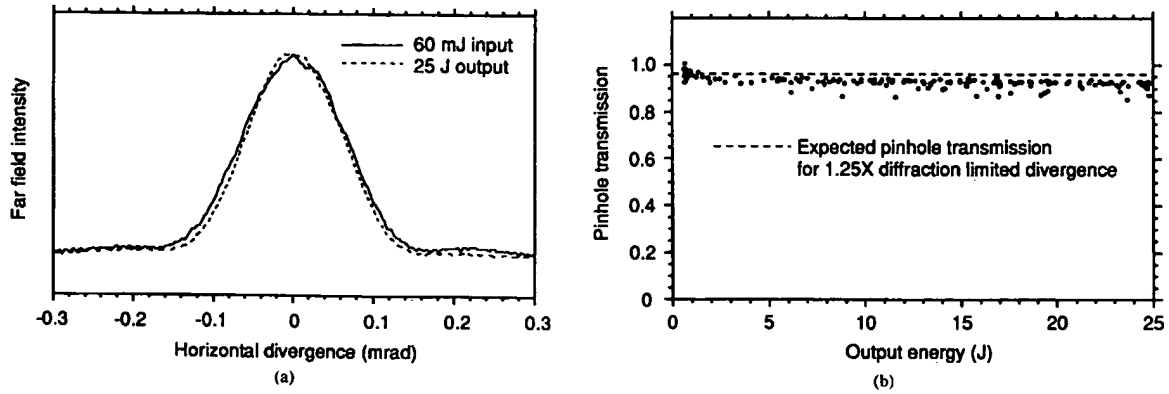

Fig. 13. (a) A comparison of horizontal cross sections of the far field profiles of the low energy input pulse (solid line) and the amplified output pulse (dashed line). The divergence is unchanged to within the uncertainty of the experimental measurement. (b) Transmission of a 0.5 mm aperture placed at the focus a 120 cm focal length lens. The expected transmission of this "bucket" for a 1.25× diffraction limited beam was calculated to be 96%. A transmission of 92% was measured across the range of output energies up to 25 J.

New Nd doped phosphate glass compositions are presently being investigated which exhibit increases in thermal fracture strength of up to 2.5× over that of the glasses presently in use in this system. An increase in the thermal fracture limit

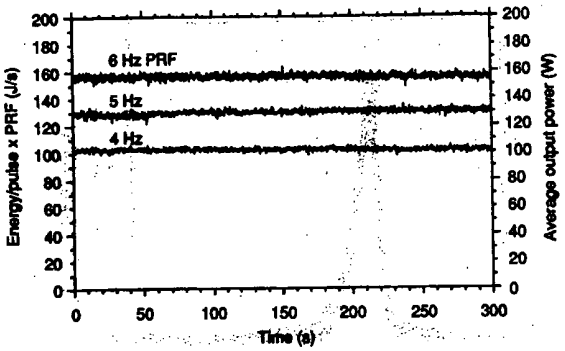

Fig. 14. Measured energy for each laser pulse (25–7 J) for continuous operation at 4, 5, and 6 Hz. The amplifier system has been operated for periods exceeding 1 hr with average output power above 150 W.

of glass slabs has also been demonstrated by ion diffusion strengthening of the laser glass [31]. Our observations in past experiments has indicated that this process of placing the glass surface in compression by exchanging lithium ions with either sodium or potassium ions often results in the introduction of passive wavefront error in the finished slab. It is anticipated, however, that the wavefront correction provided by the SBS phase conjugator can accommodate this additional distortion. Finally, it has been recently demonstrated that the pulse repetition frequency can be increased by approximately a factor of two with the same size induced optical aberrations when the flashlamp excitation of this amplifier head is replaced by diode laser array pumping [32]. It is anticipated that with these advances, the average power of a glass amplifier system of this design will increase more than three fold to 500 W.

VIII. Second Harmonic Conversion

A. Doubler Design Considerations

The frequency doubler design philosophy used for this system is best summarized by "less is better." This extends to the choice of the doubler material itself, any required auxiliary optics, and any supporting mechanical hardware. As applied to the output of a slab laser this means determining if efficient conversion is possible without any beam shaping optics intervening between the amplifier output and the frequency converter. The nonlinear material parameters that were evaluated with this consideration included: the nonlinear coefficient, the optical damage threshold, the intrinsic absorption at the fundamental and the second harmonic wavelengths, and the sensitivity of the conversion efficiency to angle, thermal distortion, and temperature. To avoid a beam shaping optical system, KD*P is the only material readily available in the required size and optical quality. Given this choice, a type II KD*P doubler was designed to achieve high conversion efficiency both on a per pulse and average power basis using the principles outlined by Eimerl [33].

A numerical solution of the coupled nonlinear wave equations shows that phase matched propagation through approximately 5 cm of KD*P is required to achieve single pulse conversion efficiency >70% with a 100 to 300 MW/cm^2 input irradiance of the fundamental. The angular sensitivity of KD*P would result in an external FWHM of 530 μrad for this length of material. Even assuming the very high beam quality and pointing stability achieved from a phase conjugated amplifier system, this still places somewhat stringent requirements on the mechanical alignment needed for high conversion efficiency. Doubler architectures using multiple crystals to reduce the sensitivity to angular misalignment have been theoretically and experimentally demonstrated [34]–[36]. With only a small increase in complexity we have increased the angular bandwidth by implementing a two crystal doubler with the optical crystal axes arranged alternating to each other, resulting in a better than a two fold increase of the angular tuning width to 1.6 mrad FWHM measured external to the crystals.

Numerical modeling of the expected average power performance based on absorption measurements [37] at the fundamental wavelength suggests that removal of the heat from the sides of the crystals to induce a transverse thermal gradient should result in <5% reduction of the conversion efficiency for a beam aspect ratio of 15:1 and for input beam average powers of 100–200 W.

B. Description of Doubler

The chosen design is a two plate alternating-Z KD*P type II doubler with one x-cut and one y-cut crystal. Presently the deuteration is 94% although levels as high as 98% can now be obtained. All surfaces are AR coated with a single sol gel layer: the first surface is optimized for the fundamental, the next two surfaces are tuned for 790 nm and the last surface is optimized for the second harmonic. The output beam shape of the zig-zag slab amplifier with its high aspect ratio of height to width is used to advantage in the design of the doubler. By choosing the long dimension to lie in the sensitive tuning plane of the crystal, the inherently smaller angular divergence associated with this dimension results in a minimized contribution to the dephasing from the diffraction-limited output beam divergence. A schematic of the doubler design is shown in Fig. 16.

The device built consists of two 2.5 cm thick bars of KD*P with input aperture dimensions of 14 × 1.4 cm. The two doubler crystals are independently mounted so that the gap between them is a few millimeters. The sides are in thermal contact with water cooled copper plates and the temperature of the water is controlled to ±0.1°C. The mechanical design allows for separate control of the angle of each crystal in the sensitive direction. In practice, each crystal is independently oriented for maximum conversion and then fine tuning is accomplished by tuning both crystals as a unit.

C. Theoretical Predictions and Experimental Conversion

The conversion efficiency of the two crystal alternating-Z doubler has been measured as a function of input energy and the results are shown in Fig. 17. The measured external

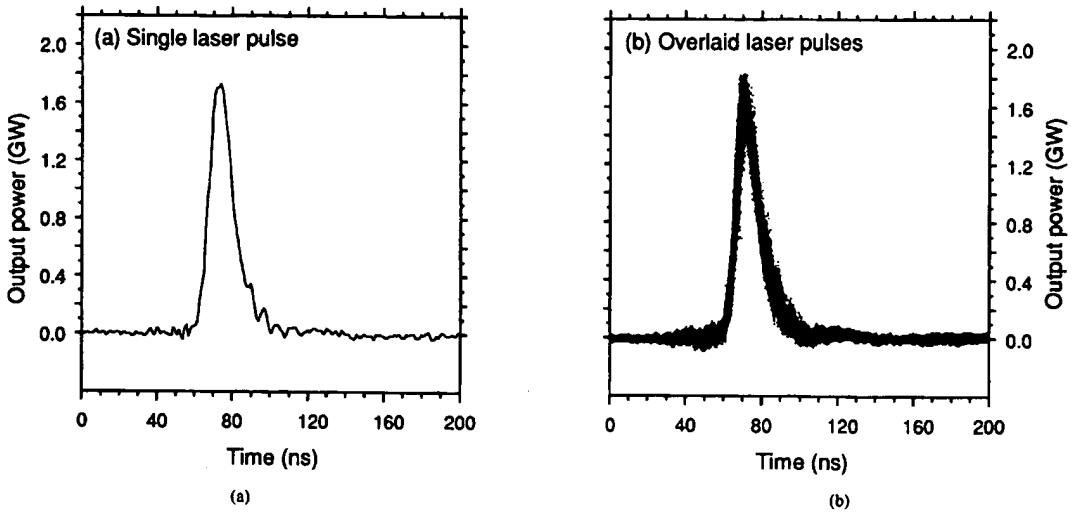

Fig. 15. The plot of (a) a single temporal waveform as well as (b) that of 1800 superimposed waveforms collected at 4 Hz. The overlaid pulses were accumulated in the infinite persistence mode of a digital storage oscilloscope.

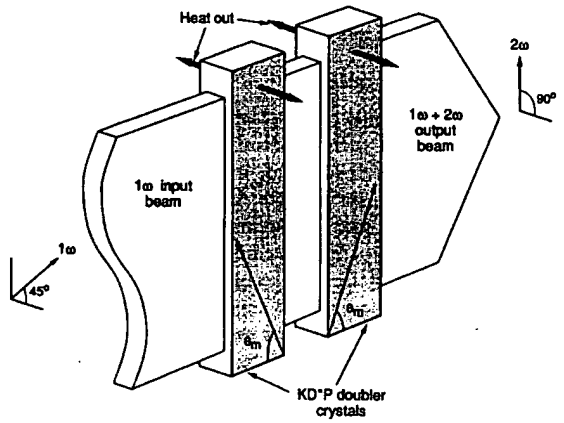

Fig. 16. Schematic of the alternating-Z KD*P second harmonic frequency converter. The unit is placed into the unshaped output beam of the regenerative amplifier after the polarization has been rotated 45° by a quartz rotator.

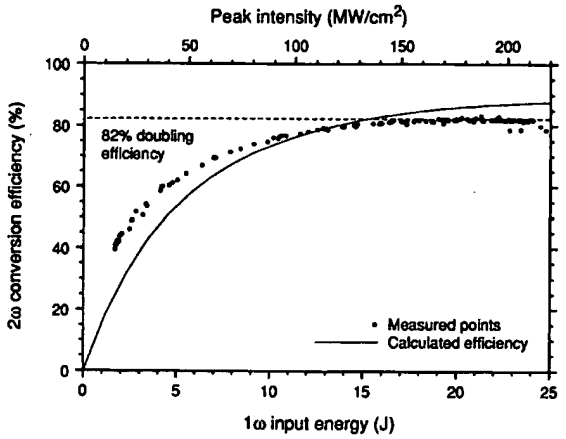

Fig. 17. Measurement of the external conversion efficiency of the two crystal alternating-Z doubler as a function of input energy in a 14 ns FWHM pulse from the amplifier. This efficiency is defined as the second harmonic energy out of the doubler assembly divided by the fundamental energy into the doubler assembly, including a 45° quartz rotator used to provide the needed polarization state of the input. Also shown on this plot (solid line) is the results of a numerical solution to the coupled harmonic equations for a spatially and temporally flat topped pulse assuming a detuning angle of 50 μrad.

conversion efficiency is plotted versus input energy in a 14 ns FWHM pulse from the amplifier. This efficiency is defined as the second harmonic energy out of the doubler assembly divided by the fundamental energy into the doubler assembly which includes a 45° quartz rotator used to provide the needed polarization state of the input. A maximum conversion efficiency of 82% is obtained corresponding to a peak irradiance of 185 MW/cm^2. Also shown on this plot is the result of a numerical solution to the coupled harmonic equations for a spatially and temporally flat topped pulse assuming a detuning angle of 50 μrad.

The overall beam shape of the 1ω output is preserved in the 2ω beam with a reduction in the beam divergence of 2×. Operation of the doubler at an average input power of 75 W yielded an output at the second harmonic of 60 W with no reduction from the single shot conversion efficiency. This performance requires only a minor optimization of the angular orientation for the steady state operation as predicted from the modeling. This high level of performance can only be achieved by maintaining high beam quality under full average power operation. The second harmonic conversion experiments were performed at an intermediate stage in the development of the full average power amplifier system. For this reason operation with the doubler at the full 150 W average input power has presently not yet been demonstrated but is expected to pose no problems.

IX. Summary of Key Amplifier Dsign Issues

In this paper, a number of design issues have been described that are important to the successful operation of a high average power amplifier system incorporating an SBS phase conjugate mirror. Of these, the key considerations can be summarized as follows.

- The amplifier design should provide very uniform pump illumination to minimize thermal distortions along the tall dimension of the slab aperture which are not averaged by the zig-zag pathway. Also, particular attention to the transition from pumped to unpumped regions at each end of the slab can minimize wavefront aberration due to incomplete averaging of index gradients and physical distortion of the end faces.
- The multipass extraction geometry should be completely image relayed to maintain a uniform irradiance spatial profile in the amplifier, to avoid loss of aberrated components of the beam wavefront before reaching the phase conjugator, and to present a smooth spatial profile to the input of the phase conjugator.
- The free propagation of the extraction beam should be minimized to reduce the irradiance distortions that result from the propagation of diffraction and thermal aberrations. In this design, the use of a double-passed refractive relay telescope places all optical surfaces near the relay image plane in the amplifier slab, minimizing potential optical damage problems that accompany folded telescope designs using reflective optics.
- The SBS phase conjugator should be operated high above threshold in order to insure the best reproduction of the high-frequency components of irradiance and phase. This also results in high energy reflectivity which minimizes the conjugator's insertion loss into the optical system and results in the accurate reproduction of the input temporal profile.
- The risetime of the leading edge of the optical extraction pulse should be longer than the acoustic relaxation time in the Brillouin medium in order to maximize the wavefront reversal fidelity when the conjugator is operated high above the stimulated scattering threshold.

X. Conclusion

We have designed and constructed a Nd:glass amplifier system incorporating a SBS phase conjugate mirror which operates at 25–30 J/pulse with a pulse width of 14 ns FWHM and a pulse repetition frequency of 6 Hz. This results in a peak power of 2 GW and an average output power that significantly exceeds 150 W. The divergence of the system is measured to be 1.25× the diffraction limit and the output can be frequency doubled with an efficiency of 82% at full average power. The laboratory prototype has proven to be an extremely reliable system and is presently in use as a laser source for a number of experimental investigations including Raman beam conversion [38], x-ray generation from laser produced plasmas [1], and high-energy SBS pulse compression [39].

The successful operation of this system demonstrates the fact that SBS phase conjugation has advanced beyond the level of an optical curiosity and is a reliable component in a high-average power laser system. The most notable improvement in laser performance resulting from the wavefront correction provided by the conjugator is the near diffraction limited output divergence. However, the phase conjugator also contributes to the reliability of the amplifier system by greatly reducing the optical alignment sensitivity, by providing interstage gain isolation between amplifier passes, and by eliminating the precise timing required to operate an intra-ring Pockels cell. Finally, we feel that the detailed considerations required for this specific amplifier design presented here are applicable in general to the design of high average power, high beam quality laser systems using SBS phase conjugation.

Acknowledgment

The authors gratefully acknowledge the valuable contributions to the optical design by J. L. Miller at Lawrence Livermore National Laboratory and to the amplifier design by J. Abate at Hampshire Instruments, Rochester, NY. We thank M. R. Hermann for developing the Frantz-Nodvik extraction model and the successful operation of the laser system would not have been possible without the excellent technical assistance of J. D. Wintemute, B. Bhachu, and W. J. Manning at Lawrence Livermore National Laboratory.

References

[1] C. B. Dane, L. da Silva, L. A. Hackel, J. Harder, D. L. Matthews, S. Mrowka, and M. A. Norton, "High average power laser-pumped 1-nm x-ray source for photolithography," in *Conf. Lasers Electro-Optics*, OSA Tech. Dig. Ser. (Opt. Soc. of Amer., Washington, DC), vol. 8, 1994, pp. 175–176.

[2] D. G. Sandler, L. Cuellar, M. Lefebvre, T. Barrett, R. Arnold, P. Johnson, A. Rego, G. Smith, G. Taylor, and B. Spivey, "Shearing interferometry for laser-guide-star atmospheric correction at large D/r_o," *J. Opt. Soc. Am.*, vol. A-11, pp. 858–873, 1994.

[3] W. S. Martin and J. P. Chernoch, "Multiple internal reflection face pumped laser," U.S. Patent 3 633 126, 1972.

[4] W. Koechner, "Slab laser with zig-zag optical path," in *Solid-State Laser Engineering*, 3rd ed. Berlin, Germany: Springer-Verlag, 1992, pp. 424–430.

[5] J. M. Eggleston, T. J. Kane, K. Kuhn, J. Unternahrer, and R. L. Byer, "The slab geometry laser—Part I: Theory," *IEEE J. Quantum Electron.*, vol. QE-20, pp. 289–301, 1984.

[6] T. J. Kane, J. M. Eggleston, and R. L. Byer, "The slab geometry laser—Part II: Thermal effects in a finite slab," *IEEE J. Quantum Electron.*, vol. QE-21, pp. 1195–1210, 1985.

[7] R. J. Gelinas, S. S. Murty, and S. K. Doss, "Thermal-stress optics modeling," *Laser Program Annu. Rep.*, Lawrence Livermore Nat. Lab., Livermore, CA, UCRL-50021, 1985, pp. 9-31–9-41.

[8] T. Kanabe, C. Yamanaka, N. Kitagawa, M. Takeda, M. Nakatsuka, and S. Nakai, "700-W Slab Nd:YAG laser," in *Conf. Lasers Electro-Optics*, OSA Tech. Dig. Ser. (Opt. Soc. Amer., Washington, DC), vol. 12, 1992, pp. 92–94.

[9] N. Hodgson, S. Dong, and Q. Lu, "Performance of a 2.3-kW Nd:YAG slab laser system," *Opt. Lett.*, vol. 18, pp. 1727–1729, 1993.

[10] B. Comaskey, G. F. Albrecht, S. C. Mitchell, C. B. Dane, and R. J. Beach, "Diode pumped one kilowatt average power slab laser," submitted to *J. Appl. Opt.*

[11] W. L. Gagnon, M. A. Summers, and J. B. Trenholme, "High-average-power solid-state glass laser: Design notes," Lawrence Livermore Nat. Lab., Livermore, CA, UCID-20921, 1986.

[12] H. Sekiguchi, H. Hara, N. Tadokoro, H. Tajima, and T. Mochizuki, "High-energy high-repetition-rate table-top glass laser system," in *Conf. Lasers Electro-Optics*, OSA Tech. Dig. Ser. (Opt. Soc. Amer., Washington, DC), vol. 12, 1992, p. 92.

[13] L. E. Zapata, R. J. Beach, C. B. Dane, P. Reichert, and L. A. Hackel, "Advanced diode-pumped, Nd:YAG slab laser for soft x-ray projection

lithography," in *Conf. Lasers Electro-Optics*, OSA Tech. Dig. Ser. (Opt. Soc. Amer., Washington, DC), vol. 8, 1994, p. 283.
[14] R. J. St. Pierre, H. Injeyan, R. C. Hilyard, M. E. Weber, J. G. Berg, R. Senn, M. G. Wickham, C. S. Hoefer, G. Harpole, and J. P. Machan, "High brightness diode-pumped solid-state laser development," in *Conf. Lasers Electro-Optics, 1993*, OSA Tech. Dig. Ser. (Opt. Soc. Amer., Washington, DC), vol. 11, 1993, pp. 274–276.
[15] L. F. Weaver, C. S. Petty, and D. Eimerl, "Multikilowatt Pockels cell for high average power laser systems," *J. Appl. Phys.*, vol. 68, pp. 2589–2598, 1990.
[16] I. M. Thomas, "High laser damage threshold porous silica antireflective coating," *Appl. Opt.*, vol. 25, pp. 1481–1483, 1986.
[17] C. B. Dane, L. E. Zapata, and L. A. Hackel, "Long pulse regenerative amplifier architecture with near diffraction-limited output divergence," in *Conf. Lasers Electro-Optics*, OSA Tech. Dig. Ser. (Opt. Soc. Amer., Washington, DC) 1993, vol. 11, p. 274.
[18] G. C. Valley, "A review of stimulated brillouin scattering excited with a broad-band pump laser," *IEEE J. Quantum Electron.*, vol. QE-22, pp. 704–712, 1986.
[19] A. A. Filippo and M. R. Perrone, "Experimental study of stimulated brillouin scattering by broad-band pumping," *IEEE J. Quantum Electron.*, vol. 28, pp. 1859–1863, 1992.
[20] J. M. Auerbach and R. L. Schmitt, "Diode-pumped monolithic Nd:YLF 1.053 mm mini-laser and its application to injection seeding," *Solid State Lasers*, in *Proc. SPIE*, vol. 1223, pp. 133–141, 1990.
[21] D. C. Hanna, B. Luther-Davies, and R. C. Smith, "Single longitudinal mode selection of high power actively Q-switched lasers," *Optoelectron.*, vol. 4, pp. 249–256, 1972.
[22] Y. K. Park and R. L. Byer, "Electronic Linewidth narrowing method for single axial mode operation of Q-switched Nd:YAG lasers," *Opt. Commun.*, vol. 37, pp. 411–416, 1981.
[23] B. Ya. Zel'dovich, N. F. Pilipetsky, and V. V. Shkunov, "Principles of Phase Conjugation," *Springer Series in Optical Sciences*, T. Thamir, Ed. New York: Springer Verlag, 1985, vol. 42, pp. 25–143.
[24] J. J. Ottusch and D. A. Rockwell, "SBS Phase Conjugation Fidelity Fluctuations," *Opt. Lett.*, vol. 16, pp. 369–371, 1991.
[25] C. B. Dane, W. A. Neuman, and L. A. Hackel, "Fidelity fluctuation in SBS phase conjugation at high input energies," in *Nonlinear Optics III*, R. A. Fisher, J. F. Reintjes, Eds., in *Proc. SPIE*, 1992, vol. 1626, pp. 308–316.
[26] C. B. Dane, W. A. Neuman, and L. A. Hackel, "Pulse-shape dependence of stimulated-Brillouin-scattering phase-conjugation fidelity for high input energies," *Opt. Lett.*, vol. 17, pp. 1271–1273, 1992.
[27] R. St. Pierre, H. Injeyan, and J. Berg, "Investigation of SBS phase-conjugation fidelity fluctuations in Freon-113," in *Conf. Lasers Electro-Optics*, OSA Tech. Dig. Ser. (Opt. Soc. Amer., Washington, DC), vol. 12, 1992, p. 180.
[28] G. J. Crofts and M. J. Damzen, "Experimental and theoretical investigation of two-cell stimulated-Brillouin-scattering systems," *J. Opt. Soc. Am. B*, vol. 8, pp. 2282–2288 1991.
[29] W. L. Smith, "Nonlinear refractive index," *Handbook of Laser Science and Technology*, M. J. Weber, Ed. Boca Raton, FL: CRC Press, Inc., 1986, vol. 3, pp. 259-264.
[30] L. M. Frantz and J. S. Nodvik, "Theory of pulse propagation in a laser amplifier," *J. Appl. Phys.*, vol. 34, pp. 2346–2349, 1963.
[31] J. E. Marion, "Strengthening of laser slabs," *Laser Progr. Annu. Rep.*, Lawrence Livermore Nat. Lab., Livermore, CA, UCRL 50021-87, 1987.
[32] G. Dube, H. Morris, T. Dellamano, J. Hollister, J. Powers, L. Long, A. Reynolds, J. Abate, E. Miller, and J. Forsyth, "700 kilowatt diode pumping system," post-deadline submission, in *Conf. Lasers Electro-Optics*, CPD7, Baltimore, MD, May 2–7, 1993.
[33] D. Eimerl, "High average power harmonic generation," *IEEE J. Quantum Electron.*, vol. QE-23, pp. 575–592, 1987.
[34] V. D. Volosov, A. G. Kalintsev, and V. N. Krylov, "Suppression of degenerate parametric processes limiting frequency-doubling efficiency of crystals," *Sov. J. Quantum Electron.*, vol. 6, pp. 1163–1167, 1976.
[35] D. Eimerl, "Quadrature frequency conversion," *IEEE J. Quantum. Electron.*, vol. 23, pp. 1361–1371, 1987.
[36] L. D. Siebert, N. K. Moncur, W. W. Lawrence, R. J. Masers, R. P. Johnson, M. B. Byers, "Multiple-crystal high-effiency frequency conversion for long-pulse lasers," in *Conf. Lasers Electro-Optics*, OSA Tech. Dig. Ser. (Opt. Soc. Amer., Washington, DC), vol. 14, 1987, pp. 258–259.
[37] C. A. Ebbers, J. A. Happe, N. D. Nielsen, and S. P. Velsko, "Absorption at 1.06 μm in Highly Deuterated KDP," *Appl. Opt.*, vol. 31, pp. 1960–1964, 1992.
[38] M. R. Herman, M. A. Norton, L. A. Hackel, and D. Twede, "Efficient high power Stokes and anti-Stokes Raman frequency generation via polarization tuning enhancement," in *Conf. Lasers Electro-Optics*, OSA Tech. Dig. Ser. (Opt. Soc. Amer., Washington, DC), vol. 11, 1993, p. 392.
[39] C. B. Dane, L. A. Hackel, and W. A. Neuman, "High energy pulse compression," *IEEE J. Quantum Electron.*, vol. 30, pp. 1907–1915, 1994.

C. B. Dane was born in Dalhart, TX, on August 8, 1961. He attended high school at the Escola Pan Americana da Bahia in Salvador, Brazil. He received the B. S. degree in chemistry and mathematics from Wayland Baptist University, Plainview, TX, in 1983. He received the M.A. and Ph.D. degrees in physical chemistry from Rice University, Houston, TX, in 1986 and 1987, respectively. His thesis work involved the high resolution infrared laser spectroscopy of transient free radical molecules.

From January 1988 to May 1990 he was a research associate with the Department of Electrical and Computer Engineering, Rice University where he worked on the scaling of the e-beam pumped XeF(C→A) laser to high energy/pulse, high repetition frequency, and ultrahigh peak power. Since that time he has worked as a physicist in the Lawrence Livermore National Laboratory Laser Program. His primary interests and research activities now include high average power solid state laser systems incorporating nonlinear wavefront correction, SBS phase conjugation and pulse compression, nonlinear frequency conversion, Raman wavelength conversion, stimulated thermal scattering, and the laser generation of x-rays for photolithography.

L. E. Zapata received his B.A. degree in physics at Washington University in St. Louis, Missouri in 1975. He did his graduate work in engineering physics at the University of Florida, Gainsville. His thesis work for the M.S. degree involved applying time-resolved nuclear spectroscopy techniques to study the structure of semiconductors. He received the Ph.D. degree in 1981 for his work measuring the lifetimes of nuclear pumped excimer molecules.

From 1980 to 1986, he was associate professor of physics at Miami University, under assignment at NASA-Langley where he did innovative experimental work on solar-pumped lasers. In 1987, he joined the Laser Program at Lawrence Livermore National Laboratory where his activities have included the development of high brightness solid state lasers.

W. A. Neuman was born in Pittsburgh, PA on August 14, 1960. He received the B.S. degree in nuclear engineering in 1982 from the Pennsylvania State University. After working at the Westinghouse Electric Corp. with the Advanced Energy Systems Division he went to the University of Arizona and received a Ph. D. in Nuclear Engineering in 1988.

From 1986 to 1988, he was a staff research assistant at the Los Alamos National Laboratory working in the areas of plasma physics and atmospheric propagation of light. In 1988, he began employment at the Idaho National Engineering Laboratory where his work concentrated on the development of nuclear pumped lasers. From 1991 until 1993, he worked under a collaborative arrangement at the Lawrence Livermore National Laboratory and in 1993 he joined the staff at LLNL. His work at the LLNL has included developing numerical modeling techniques to study stimulated Brillouin scattering for phase conjugation and pulse compression, solid state laser pumping and energy dynamics, and beam propagation analysis. His current work also includes developing optical parametric oscillators to produce mid-IR radiation for remote sensing applications.

M. A. Norton received the A. B. degree in Physics from Emmanuel College and an M. S. and Ph. D. degree in Physics from The University of Arizona.

In 1978, she joined M.I.T. Lincoln Laboratory where her research centered on adaptive optics and atmospheric propagation effects. In 1987, she joined Lawrence Livermore National Laboratory where her research interests have included nonlinear optics, solid state lasers and high average power devices.

L. A. Hackel was born in Little Chute, WI on October 14, 1949. He received the B.S. degree in 1971 in applied math and physics from the University of Wisconsin, Madison. He was granted a Defense Education Act Fellowship for graduate work at the Massachuset ts Institute of Technology, Cambridge, MA and received the M.S. degree in 1973 and the Sc.D. degree in 1974. His doctoral dissertation involved the development of frequency stabilized lasers and molecular beam techniques for very high resolution spectroscopy.

From 1974 to 1976, he was a staff member of the MIT Research Laboratory of Electronics. In 1976, Dr. Hackel began employment with the Lawrence Livermore National Laboratory working on laser isotope separation. Here he developed multistep photoionization processes for a number of atomic elements and then developed high mass-throughput electron beam vaporizers and collector systems. In 1987, he began work for Lockheed missles and Space Company, Sunnyvale, CA as a group leader for systems engineering for a Strategic Defense Initiative space program. He returned to Lawrence livermore in 1989 to work on solid state laser systems. His current work includes high average power flash lamp and diode pumped solid state laser systems. His current work includes high average power flash lamp and diode pumped solid state lasers, phase conjugation for high beam quality, and nonlinear frequency conversion including the generation of UV and x-rays for microlithography.